

3D vibration control of flexible manipulator by inverse systems using inner and outer decomposition

Minoru Sasaki^a, Daiki Meno^b, Muguro Joseph^{a, c}, Mizuki Takeda^b, Waweru Njeri^c and Kojiro Matsushita^b

^aIntelligent Production Technology Research & Development Center for Aerospace, Gifu University, Tokai National Higher Education and Research System, 1-1 Yanagido, Gifu 501-1193, Japan, E-mail: sasaki@gifu-u.ac.jp

^bDepartment of Mechanical Engineering, Faculty of Engineering, Gifu University, 1-1 Yanagido, Gifu 501-1193, Japan.

^cCenter for Robotics and Biomedical Engineering, Dedan Kimathi University of Technology, Nyeri

Abstract

This paper presents vibration control of a flexible manipulator that has two links and three degrees of freedom and that performs three-dimensional motion and verified the suppression of vibration in three-dimensional space using an actual manipulator using an inverse system. At present, industrial robots are required to increase the speed of operation in order to reduce the weight of the robot and improve the work efficiency for the purpose of energy saving and cost reduction. However, if the weight of the arm is reduced, the rigidity is inevitably low, which causes vibration of the entire arm. In addition, if the operation speed is increased, vibration will occur in the arm even if the robot is highly rigid. For these reasons, the development of a control method that takes into account the flexibility of the manipulator is an important issue, and various studies have been conducted, but the study of vibration suppression in three-dimensional motion is also difficult to model and control. One of the approaches is to suppress vibration using an inverse system. Previous studies have shown that vibration suppression is possible with the inverse system. Problems such as the resonance frequency component in the torsional direction remaining and overshooting with respect to the target angle remain. Therefore, in this research, we aimed to improve the vibration suppression performance in the torsional direction and the tracking performance to the target angle, which remained as issues in the conventional research.

First, we applied and verified a new inverse system design method. We constructed a stable inverse system using inner and outer decomposition for the unstable zero of the flexible manipulators and confirmed the effectiveness for vibration suppression by simulation. After that, the vibration suppression performance of the controller was confirmed in a mounting experiment, and it was confirmed that it was effective in suppressing vibration in the torsion direction and the motor drive direction. In addition, it was confirmed that overshoot with respect to the target angle, which was the subject of conventional research, did not occur. From the results, it was confirmed that the proposed inverse system is effective for vibration control of the flexible manipulator that moves in three dimensions.

Keywords: flexible manipulator, vibration control, inverse system, inner and outer decomposition.

Introduction

1.1 Research background

One of the design indexes for industrial robots is to improve the positioning accuracy of the arm tip. In the past, in order to achieve this, it was a common method to increase the structural rigidity of the robot arm. However, increasing the rigidity leads to an increase in weight, which causes many disadvantages in terms of energy consumption and cost. From this point of view, it is desired to reduce the weight of the arm for the purpose of energy saving and cost reduction. However, if the weight of the arm is reduced, the rigidity will decrease, and the vibration and deflection of the arm itself will be noticeable. Also, even in a high-rigidity robot, if the movement becomes high speed, the vibration of the arm part cannot be ignored. In this way, in industrial robots, the flexibility inherent in the components cannot be ignored in order to reduce the weight of the arm and realize high-speed operation, and it is necessary to give due consideration to it [1].

On the other hand, for robots used in outer space, it is desirable to reduce the weight of the robots to be mounted as much as possible from the viewpoint of restrictions on the load weight of launch rockets and space shuttles and cost reduction at the time of launch. In addition, the influence of gravity is small in outer space where robots work, and rigidity is not required to support their own weight, so weight reduction is being actively promoted. For these reasons, it is necessary to consider the flexibility of the components [2]. Against the above background, research on the suppression of vibration due to elastic deformation of flexible manipulators is being actively conducted.

1.2 Conventional research

1.2.1 Conventional research on flexible arms

Research on flexible arms can be broadly divided into model-based control and model-free control. Dynamics-based models are commonly used in model-based control. This is a method that focuses on the dynamics of the distributed constant system of the flexible structure and obtains the solution of the equation of motion related to vibration by solving the partial differential equation. There are other methods such as modeling using the finite element method [3] [4] [5]. Many documents limit the motion of the flexible arm to a two-dimensional plane and model it. In recent years, it has become possible to model flexible robot arms relatively easily by improving the computing power of personal computers and the sophistication of computer algebra software and simulation software. On the other hand, model-free control does not require a mathematical model to be controlled. In Ref. [6], it is theoretically and experimentally that direct strain feedback (DSFB) control, which extracts the strain value from the strain sensor attached to the link and feeds it directly to the input to the servomotor, is effective for vibration control. Is shown. After that, Takeuchi showed that DSFB control is also effective for the three-dimensional motion of the flexible manipulator [7].

However, despite long-standing research on flexible arms, there are few research cases that consider three-dimensional vibration.

1.2.2 Conventional research on inverse systems

The inverse system is the inverse problem of finding the control input $u(t)$ so that the output $y(t)$ of the system matches the desired response $r(t)$ [7]. As shown in Fig. 1.1, when the control target is G , \hat{G} corresponds to the inverse system. The inverse system that comes before the controlled object as shown in the figure is called the right inverse system. Hereinafter, what is called an inverse system refers to a right inverse system.

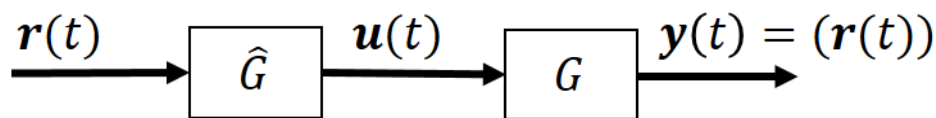


Fig. 1.1 Inverse system.

Research on the design method of the inverse system has been actively conducted since the 1960s. In control engineering, a lot of research has been done with the proposal of the construction method of the inverse system for the system of one input and 1 output in the transfer function representation.

Later, Silverman's configuration algorithm and the inverse system by Sain and Massy were proposed as the method of constructing the inverse system for the multi-input multi-output system. These show how to design an inverse system when the controlled system is represented by a time-invariant state-space model. Since the above inverse system requires an ideal differentiator to faithfully reproduce the response characteristics of the system, there are problems such as amplifying noise. Therefore, a low-frequency pass-through inverse system was proposed, which gave up the reproduction of high-frequency components and improved the stability of the system. Since the low pass type inverse system does not require a differentiator, it is considered to be an effective method in terms of practical use [8]. As mentioned above, stability is important in the configuration of the inverse system. If G , which is the controlled system, is stable, that is, it does not have a pole where the real part is positive, and it does not have an unstable zero point where the real part is positive, it is easy to configure the inverse system. Can be done. However, when it has an unstable zero point such as a dead time system, it is necessary to devise when configuring the inverse system. Many methods have already been proposed, such as a method using a parallel feedforward compensator and inner / outer decomposition, for the inverse system configuration when there is an unstable zero point [9]. A parallel feedforward compensator is a method of attaching a compensator so that it is parallel to the controlled system. By regarding the compensator and the control target added in parallel as one control target system, it is possible to construct a stable inverse system by making it a minimum phase system without unstable zeros [11]. Inner-outer decomposition, which plays an important role in robust control, is also applied to the inverse system. Inner-outer decomposition is a method of decomposing the controlled system into an outer function that is stable and does not have a zero in the right open half-space, and other inner functions. At that time, a stable control system can be designed by making the outer function that does not have an unstable zero point an inverse system [12].

1.2.3 Vibration control using an inverse system

In Ref. [19], the inverse system described above is applied to the vibration control of the flexible manipulator. Since the flexible manipulator is a dead time system, it has an unstable zero when it is used as a state space model. On the other hand, we divided it into external dynamics and internal dynamics, and controlled the unstable part as an inverse system by stabilizing it by state feedback and showed its effectiveness. However, when operated at high speed, there are still problems that the vibration in the torsion direction and the vibration in the in-plane direction cannot be partially suppressed and that the overshoot with respect to the target angle is caused.

1.3 Research purpose

In this study, we control the flexible manipulator using an inverse system and distortion feedback for the purpose of suppressing vibration in three-dimensional space.

First, we will construct a new inverse system aiming at improving vibration suppression performance and target tracking performance compared to conventional research. In the conventional research, the controller was stabilized by feeding back the unstable pole generated in the inverse system. However, in Silverman's construction algorithm used here, the inverse system itself has a differentiator. When actually controlling, an ideal differentiator cannot be constructed, and the system tends to become unstable when noise or a steep input occurs, so it cannot be said to be practical. Therefore, in the conventional research, the cutoff frequency is set to a low value to prevent excessive input. Therefore, many signals are cut, and there is a possibility that signals with frequencies important for control are also canceled. In addition, the pole arrangement by feedback is performed to stabilize the inverse system, but this may reduce the effect of pole-zero cancellation. In addition, it is necessary to select the optimum feedback gain by trial and error. As a result, in the conventional research, problems such as overshoot with respect to the target angle and some vibration components in the torsional direction could not be suppressed remained.

Therefore, in this study, we construct a stable inverse system by inner-outer decomposition, which is often used in robust control, for the state-space model of a flexible manipulator with an unstable zero. By using the inner / outer decomposition, it is possible to keep the gain of the controlled object and the inverse system equal. In addition, since the outer function constructed by inner-outer decomposition has the same order of numerator and denominator, the inverse system is proper and does not have a differentiator, so it is easier to put into practical use than the conventional method. In addition, unlike the conventional method, there is no process to determine the feedback gain, so there is an advantage that it can be systematically performed without constructing a controller by trial and error. The performance verification of the inverse system by the proposed method is performed by simulation and mounting experiment. Next, we will conduct an experiment of vibration control by distortion feedback and confirm its vibration suppression performance. Next, we verify the effectiveness of the proposed method in this study by performing two-degree-of-freedom control that combines an inverse system and

distortion feedback. Finally, for the purpose of orbit control, we will verify whether the proposed method of this study is also effective in suppressing vibration at the tip.

Development of control system

2.1 Introduction

In this chapter, the configuration of the flexible manipulator to be controlled, the experimental equipment, and the experimental method are described, and the modeling of the flexible manipulator and the construction method of the inverse system, which is the proposed method of this research, are described.

2.2 Control target configuration

2.2.1 Flexible manipulator

Figure 2.1 shows the overall view of the flexible manipulator to be controlled. The flexible manipulator has 2 links and 3 degrees of freedom. The material of link 1 is stainless steel (SUS304), and the material of link 2 is aluminum (A2017). The material is different because the load on Link 1 is large and aluminum causes plastic deformation.

At the bases of links 1 and 2, strain gauges are attached by the 2-gauge method in the direction of rotation of Joint2 and Joint3 (hereinafter referred to as the in-plane direction) and in the direction orthogonal to it (hereinafter referred to as the out-of-plane direction). There is. In addition, a strain gauge is attached to the base of link 1 by the 4-gauge method to measure torsional strain. The reason for using the 4-gauge method here is that the torsional strain is a small numerical value compared to the vibration in the in-plane and out-of-plane directions, so the voltage generated by the strain is amplified and a more accurate numerical value is measured.

Joint1 is mounted perpendicular to the ground, and Joint2 and Joint3 are mounted horizontally to the ground, making it possible to move in three dimensions. The rotation angle of Joint1 is ± 180 [deg], and the rotation angle of Joint2 and Joint3 is ± 90 [deg]. Each Joint uses a DC servo motor with a built-in line driver type optical encoder with an output pulse of 1000 [Pulse / Rev], and a harmonic drive with a reduction ratio of 1/100 is used between the motor and the rotating shaft. It has been done. In addition, a cast iron cylinder with the same mass as each motor is attached to maintain the balance between the left and right sides.

A 170 [g] weight is attached to the tip of the arm, and vibration and deformation are noticeable on each link. Table 2.1 shows the physical parameters of each part.

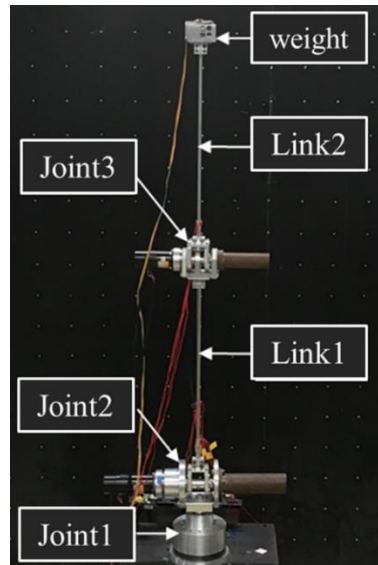


Fig. 2.1 Flexible manipulator.

2.2.2 Experimental equipment

Figure 2.2 shows the configuration of the experimental equipment used this time. The control program creates a model using Simulink, which is one of the functions of the control system design support tool MATLAB (manufactured by The MathWorks) installed on the PC (OS: Windows 10, manufactured by Microsoft). Generate C code from the created model and download it to MicroLabBox (manufactured by dSpace). Data input / output is sent to a speed-controlled servo amplifier (DA2 series manufactured by Sanyo Electric Co., Ltd.) through the D / A converter built into the MicroLab Box to operate the servo motor. At this time, the rotation angle of the servo motor is fed back from the encoder attached to the motor through the counter board. In addition, the sensor voltage of the distortion gauge attached to the base of the link is amplified by a dynamic distortion meter (DPM713B, DPM913B manufactured by Kyowa Electric Co., Ltd.) as a signal amount via a bridge circuit, and the A / D converter built into the MicroLab Box. Is input through. The maximum input voltage that can be input from the MicroLabBox is ± 10 [V], and the rotation speed of the DC servomotor with respect to the input voltage is $1000/3$ [rpm / V]. The cutoff frequency of the dynamic strain meter is set to 30 [Hz] for both bending strain and torsional strain. This is because the vibration mode, which is the main cause of vibration in the flexible manipulator, appears below 30 [Hz]. In addition, the measurement range is 2000 [$\mu\epsilon$] and the calibration value is $2000/2$ [$\mu\epsilon$ / V], and the following experiment is performed.

2.2.3 Experimental settings

The initial posture of the flexible manipulator is perpendicular to the ground. The input is a square wave with a period of 20 [s]. At the same time as the start of the experiment, the attitude of the flexible manipulator changes when the voltage corresponding to the target angle is input to each of the Joint1, Joint2, and Joint3 motors. After that, after 10 [s], the posture returns to the same vertical posture as the start of the experiment. The experiment ends 10 [s] after returning to the original posture, that is, 20 [s]

after the start of the experiment. In this experiment, the sampling frequency is set to 10 [kHz].

2.3 Modeling of flexible manipulator

In this section, we will create a linear model of the flexible manipulator necessary for constructing an inverse system and a nonlinear model for verification by simulation. In this research, we create a linear model and a non-linear model of the flexible manipulator to be controlled using Maplesim™ (manufactured by Maple), which is software capable of modeling and simulation.

Since ordinary industrial robots have high rigidity, dynamic elements such as vibration are minute, and they are almost negligible in modeling. However, since the flexible manipulator has low rigidity, the equation of motion of the joint and the link part and the equation of motion regarding the vibration generated in the link part cannot be ignored in the modeling. Furthermore, the equations that represent three-dimensional motion are complicated and esoteric. Therefore, in this study, Maplesim™, which enables equation-based modeling, is used to model the flexible manipulator. Maplesim™ enables integrated modeling and simulation of physical systems across multiple physical domains, such as electrical circuits, multibody, and one-dimensional mechanicals. In addition, by linking with Maple ^
TM, which is computer algebra software, it is possible to generate mathematical models such as controlled equations and linear models, and to optimize the models. In Maplesim™, the analysis result of the controlled model can be visually confirmed by the automatic animation creation function of the multibody model. Furthermore, the designed model can be used as an S-function block that can be used in the control system design support tool Matlab / Simulink. This function makes it possible to easily simulate the designed controller.

Figure 2.2 shows the created 3D model. The physical parameters of each part were determined with reference to those described in the specifications. The gravitational acceleration was $9.81[\text{m/s}^2]$, and it was assumed that there was no influence of air resistance or heat. The model created this time elastically deforms in the x-axis direction and the z-axis direction. In the following, the details of the model will be described separately for the mechanical model and the electrical model.

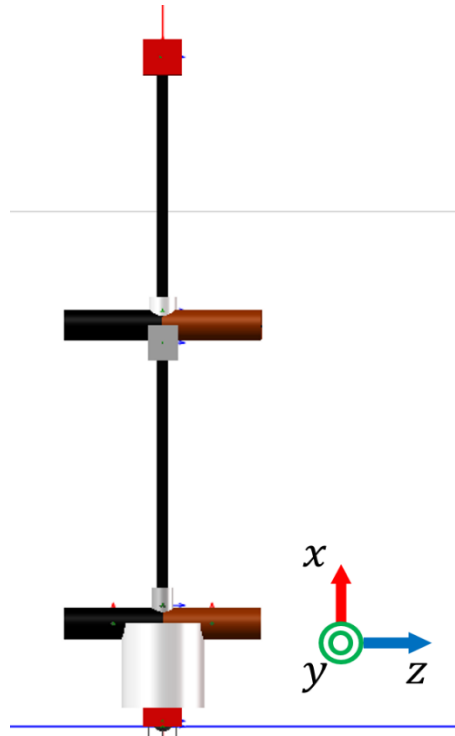


Fig. 2.2 Maplesim.TM 3-D Visualization model.

2.3.3 Linear model

Since the inverse system, which is the proposed method, is created based on the time-invariant state-space model, it is necessary to linearize the nonlinear model of the flexible manipulator created so far. Therefore, a state space model is created using Maplesim.[^] TM and Linearize, which is one of the functions of Maple. The input of the state space model was the target angle of each motor, and the output was the angular displacement and torsional distortion of each motor and the in-plane distortion of Link1 and Link2. Each is defined as a variable as Eq. (2.13) and Eq. (2.14). The state variable is Eq. (2.15).

$$u(t) = [\theta_{d1} \quad \theta_{d2} \quad \theta_{d3}]^T \quad (2.13)$$

$$y(t) = [\theta_1 \quad \theta_2 \quad \theta_3 \quad \varepsilon_{torsion} \quad \varepsilon_{in1} \quad \varepsilon_{in2}]^T \quad (2.14)$$

$$x(t) = [x_1(t) \quad x_2(t) \quad \dots \quad x_{16}(t) \quad x_{17}(t)]^T \quad (2.15)$$

Where the variables shown in Eq. (2.15) are as follows.

$i_i(t)$: Current flowing through the motor

$\varepsilon_{ij}(t)$: Strain of each link

$\theta_i(t)$: Motor rotation angle

$$\begin{aligned} x_1(t) &= i_1(t) & x_2(t) &= i_2(t) & x_3(t) &= i_3(t) \\ x_4(t) &= \varepsilon_{11}(t) & x_5(t) &= \dot{\varepsilon}_{11}(t) & x_6(t) &= \varepsilon_{12}(t) \\ x_7(t) &= \dot{\varepsilon}_{12}(t) & x_8(t) &= \varepsilon_{21}(t) & x_9(t) &= \dot{\varepsilon}_{21}(t) \\ x_{10}(t) &= \varepsilon_{22}(t) & x_{11}(t) &= \dot{\varepsilon}_{22}(t) & x_{12}(t) &= \theta_1(t) \end{aligned}$$

$$\begin{aligned}
 x_{13}(t) &= \dot{\theta}_1(t) & x_{14}(t) &= \theta_2(t) & x_{15}(t) &= \dot{\theta}_2(t) \\
 x_{16}(t) &= \theta_3(t) & x_{17}(t) &= \dot{\theta}_3(t)
 \end{aligned}$$

2.3.4 Model evaluation by simulation

Verify the validity of the models described so far. The evaluation targets are the nonlinear model and the linear model described so far, and the evaluation is performed by comparing with the actual measurement data obtained in the actual manipulator.

Fig. 2.5 shows the angular response when the target angle of each motor is operated as a step response of 20 [deg], and Fig. 2.6 show the strain results. Although the convergence speed is different from Fig. 2.5, it converges to the same value in all Joints. In addition, from Fig. 2.6, the steady-state strains are the same in the in-plane direction of link 1 and link 2. It can be seen that the vibration characteristics also match. From the above, it can be evaluated that the model created this time is appropriate in terms of angular response and vibration characteristics. From now on, the controller will be designed based on the linear model created in this chapter.

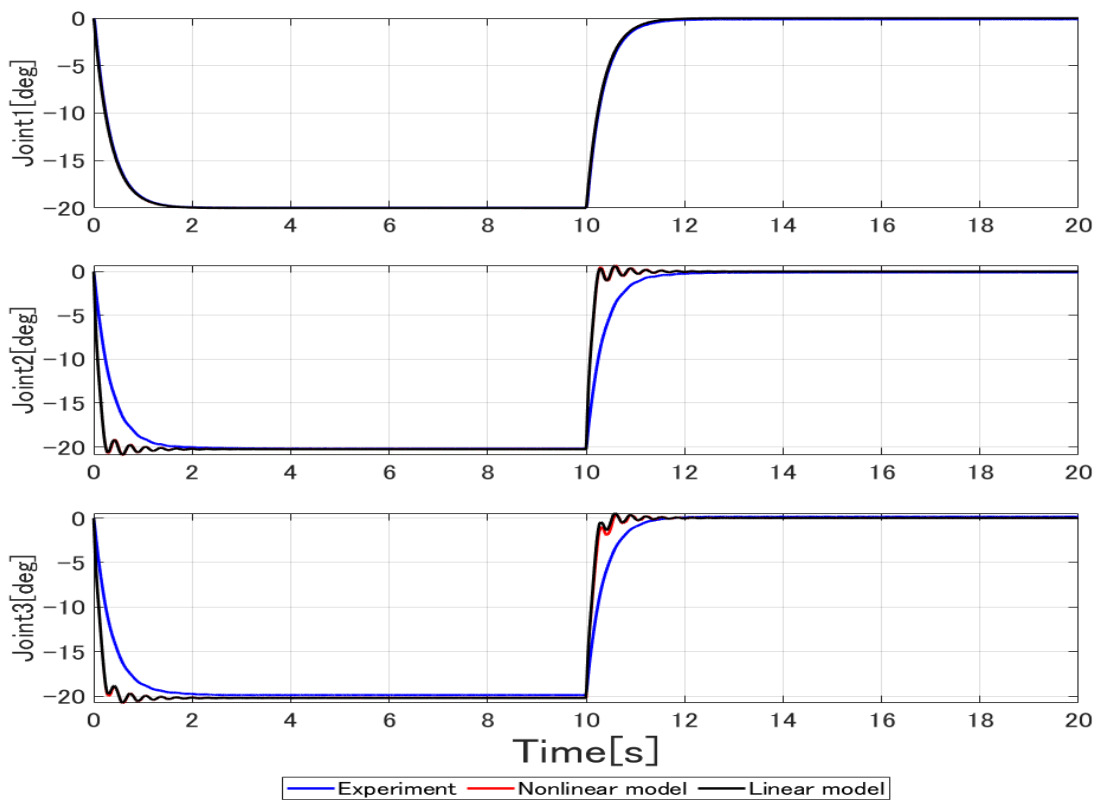


Fig. 2.5 Comparison of angle response.

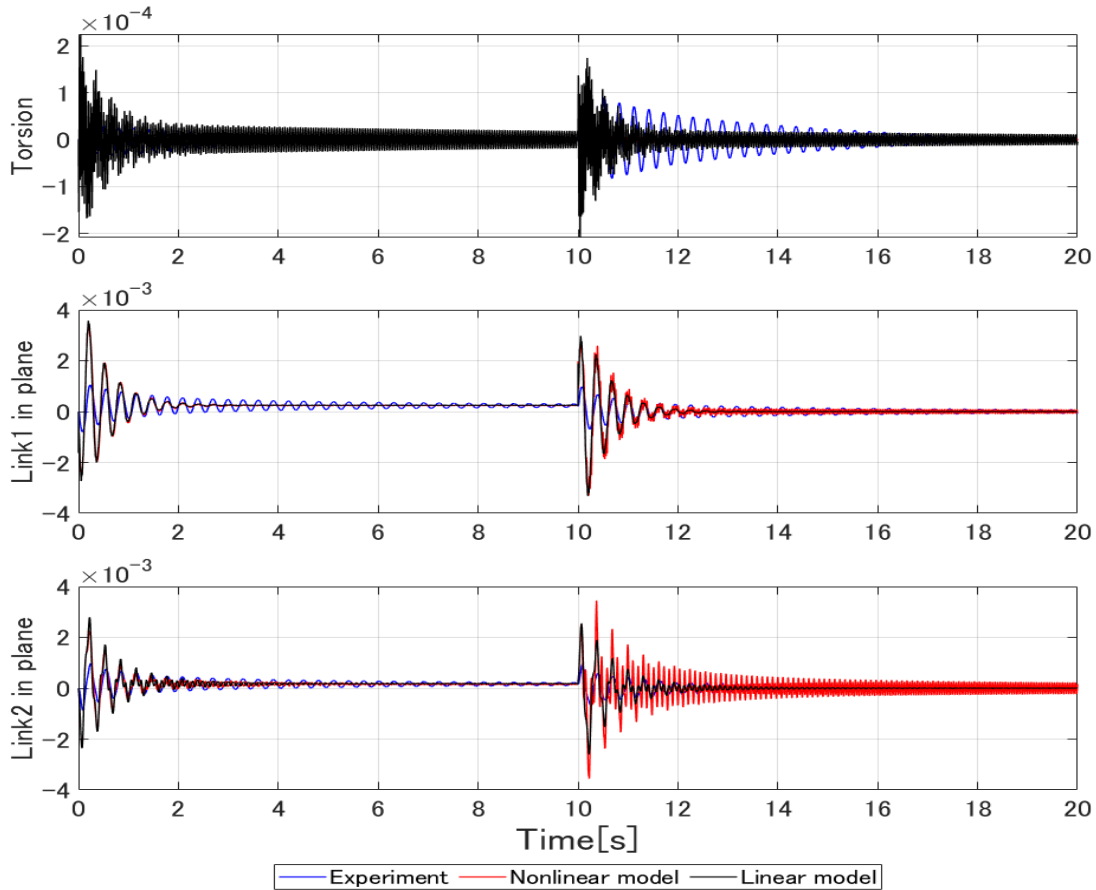


Fig. 2.6 Comparison of strain response.

2.4 Inverse system configuration of flexible manipulator

This section describes the method of constructing the controller used in this study.

The explanations of symbols and terms used in this paper are summarized below.

\mathbb{R} : Real number set

\mathbb{C} : Imaginary set

$\mathbb{R}^{m \times p}$: Real coefficient matrix set of m rows and p columns

$$\left[\begin{array}{c|c} A & B \\ \hline C & D \end{array} \right] : \text{State space representation } C(sI - A)^{-1}B + D$$

$$\left\{ E, \left[\begin{array}{c|c} A & B \\ \hline C & D \end{array} \right] \left[\begin{array}{c|c} A & B \\ \hline C & D \end{array} \right] \right\} : \text{Descriptor - style state - space representation}$$

Finite zero: Zero that exists at the position where $s \neq 0$

Infinite Zero : Zero where $s = \infty$

A^\dagger : Generalized inverse of matrix A of $m \times n$

2.4.1 Characteristics of linear model

Here, the characteristics of the linear model of the created flexible manipulator will be considered based on the frequency characteristics and the pole-zero map and will be prepared for the inverse system configuration.

Next, we describe the poles and zeros of the linear model of the flexible manipulator. Figure 2.14 shows the polar zero table of the linear model created. It can be seen from the table that there are no finite zeros. This is thought to be because systems with inconsistent numbers of inputs and outputs generally do not have finite zeros and have many infinite zeros [30]. Regarding the infinite zero, when the inverse system is used, it becomes a pole with a finite value, so it is necessary to consider the construction method of the inverse system in consideration of this. In addition, it is highly possible that the real part of the infinite zero is smaller than the real part of the pole that is far from the imaginary axis. Inner-outer decomposition is used when designing a stable inverse system, but the general Riccati equation normally used here is a condition that has no zero on the imaginary axis. When using numerical calculation processing software, there is a high possibility that a solution cannot be obtained if there is a zero that is extremely close to the imaginary axis as opposed to other poles and zeros. Therefore, it is necessary to perform inner-outer decomposition using a method other than the usual Riccati equation.

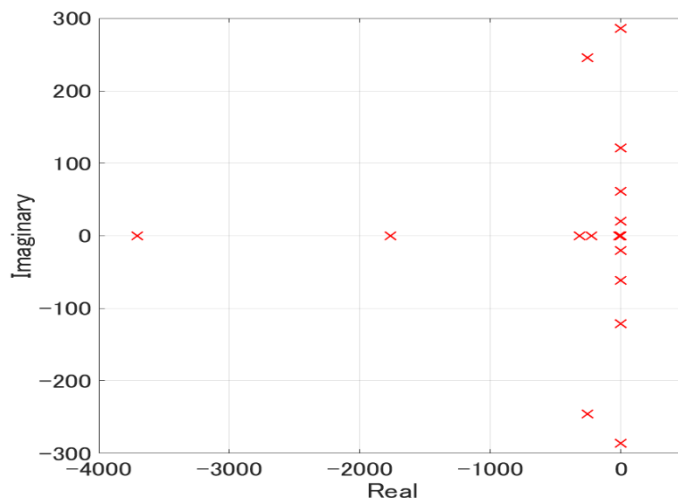


Fig. 2.14 Pole-Zero map.

From the above consideration, the characteristics of the linear model that should be considered when creating the inverse system this time are summarized in the following three.

- (I) $\text{rank}(D) < p \cap p > m$.
- (ii) Has an infinite zero.
- (iii) It has a zero on the imaginary axis including the point at infinity or near the imaginary axis.

2.4.2 Inverse system configuration method of conventional research

In the previous research, we used a model in which the output of the linear model used this time was

reduced to three, that is, $p = m$.

Let the given state space model be Eq. (2.16) and Eq. (2.17).

$$\dot{x}(t) = Ax(t) + Bu(t) \tag{2.16}$$

$$y(t) = Cx(t) \tag{2.17}$$

Where each character is defined as follows.

$$A \in \mathbb{R}^{n \times n}$$

$$B \in \mathbb{R}^{n \times p}$$

$$C \in \mathbb{R}^{p \times n}$$

However, A , B , and C are time-invariant, respectively. In order to proceed with the following discussion, the variables l and r are newly defined as follows.

$$C = \begin{bmatrix} C_1 \\ \vdots \\ C_p \end{bmatrix}$$

$$r \triangleq [r_1 \ r_2 \ \dots \ r_p]^T \text{ if } C_i A^l B = 0, \forall l < r_i - 1; 1 \leq i \leq p$$

Eq. (2.18) is obtained by differentiating the i th output to the r_i order.

$$y^{(r_i)}(t) = C_i A^{(r_i)} x(t) + C_i A^{(r_i-1)} B u(t) \tag{2.18}$$

When this is done for all outputs, Eq. (2.19) holds.

$$y^{(r)}(t) = A_x x(t) + B_y u(t) \tag{2.19}$$

where, each variable is as follows.

$$y^{(r)}(t) \triangleq \begin{bmatrix} y_1^{(r_1)}(t) \\ \vdots \\ y_p^{(r_p)}(t) \end{bmatrix}$$

$$A_x \triangleq \begin{bmatrix} C_1 A^{(r_1)} \\ \vdots \\ C_p A^{(r_p)} \end{bmatrix}$$

$$B_y \triangleq \begin{bmatrix} C_1 A^{(r_1-1)} B \\ \vdots \\ C_p A^{(r_p-1)} B \end{bmatrix}$$

At this time, in order to satisfy $\det(B_y) \neq 0$, Eq. (2.20) is transformed to obtain the following equation.

$$u(t) = B_y^{-1} [y_d^{(r)}(t) - A_x x(t)] \tag{2.20}$$

Furthermore, at this time, there exists a transformation matrix $T \in \mathbb{R}^{n \times n}$ that satisfies the following equation.

$$x(t) = T \begin{bmatrix} \xi(t) \\ \eta(t) \end{bmatrix}^T \tag{2.21}$$

$$\xi(t) = [y_1(t) \ y_1(t) \ \dots \ y_1^{(r_1-1)}(t) \ \dots y_p(t) \ \dot{y}_p(t) \ \dots \ y_p^{(r_p-1)}(t)]^T : \text{external dynamics}$$

$\eta(t)$: internal dynamics

The external dynamics shown above are variables up to the output and its r_i derivative. internal dynamics is a state variable other than external dynamics and means a variable that cannot be directly controlled by input.

Equation (2.22) and Equation (2.23) can be derived using Equation (2.21).

$$\dot{\xi}(t) = \hat{A}_1 \xi(t) + \hat{A}_2 \eta(t) + \hat{B}_1 u(t) \tag{2.22}$$

$$\dot{\eta}(t) = \hat{A}_3 \xi(t) + \hat{A}_4 \eta(t) + \hat{B}_2 u(t) \tag{2.23}$$

$$\hat{A} = T^{-1}AT = \begin{bmatrix} \hat{A}_1 & \hat{A}_2 \\ \hat{A}_3 & \hat{A}_4 \end{bmatrix} \quad \hat{B} = T^{-1}B = \begin{bmatrix} \hat{B}_1 \\ \hat{B}_2 \end{bmatrix}$$

Furthermore, the following transformation is possible based on the transformation matrix T .

$$A_x T = [A_\xi \quad A_\eta]$$

Equation (2.24) holds from the transformation matrix defined above and equation (2.20).

$$u(t) = B_y^{-1} \left[y_d^{(r)}(t) - A_\xi \xi(t) - A_\eta \eta(t) \right] \tag{2.24}$$

By substituting t Eq. (2.24) into Eq. (2.23), Eq. (2.25) can be obtained.

$$\begin{aligned} \dot{\eta}(t) &= \hat{A}_3 \xi(t) + \hat{A}_4 \eta(t) + \hat{B}_2 B_y^{-1} \left[y_d^{(r)}(t) - A_\xi \xi(t) - A_\eta \eta(t) \right] \\ &= (\hat{A}_4 - \hat{B}_2 B_y^{-1} A_\eta) \eta(t) + [(\hat{A}_3 - \hat{B}_2 B_y^{-1} A_\xi) \quad \hat{B}_2 B_y^{-1}] [\xi(t)^T \quad y_d^{(r)}(t)^T]^T \\ \dot{\eta}(t) &= \hat{A}_\eta \eta(t) + \hat{B}_\eta Y \end{aligned} \tag{2.25}$$

And Eq. (2.24) is transformed and defined as follows.

$$\begin{aligned} u(t) &= -B_y^{-1} A_\eta \eta(t) - [B_y^{-1} A_\xi \quad -B_y^{-1}] Y \\ &= \hat{C}_\eta \eta(t) + \hat{D}_\eta Y \end{aligned} \tag{2.26}$$

From the above, we obtain equations (2.27) and (2.28), which are inverse systems.

$$\dot{\eta}(t) = \hat{A}_\eta \eta(t) + \hat{B}_\eta Y \tag{2.27}$$

$$u(t) = \hat{C}_\eta \eta(t) + \hat{D}_\eta Y \tag{2.28}$$

However, at this point, the original linear model has an unstable zero, which results in an unstable inverse system. Therefore, the inverse system is stabilized by arranging the unstable poles of the inverse system on the left half-plane in the pole-zero table using state feedback. At this time, controllability of internal dynamics is guaranteed.

In the previous research, a filter was also constructed to enhance the robustness of the controller. Since the inverse system has the opposite frequency characteristics to the original system, there is a risk of enhancing the high frequency components. Therefore, the system may become unstable with an input that has a steep rise like the step response used this time. Therefore, the high frequency component is cut by adding the transfer function composed of Eq. (2.29) in series. This time, $n = 2$ and $\lambda = 0.3$.

$$f(s) = \frac{1}{(\lambda s + 1)^n} \tag{2.29}$$

2.4.3 Inner outer decomposition

Here, after organizing the definitions of inner-outer decomposition, we describe the inner-outer decomposition using the commonly used standard spectral decomposition. Next, the singular spectral decomposition applicable to this model is described, and the inner outer decomposition applicable to the properties of (i) (ii) (iii) summarized in 2.4.1 is described.

Suppose that a stable system $G(s)$ can be converted as shown in equation (2.30).

$$G(s) = G_i(s)G_o(s) \tag{2.30}$$

Where $G_o(s)$ is stable and has no zero at \mathbb{C}^+ . Also, Eq. (2.31) is satisfied.

$$|G_o(s)| = |G(s)| \tag{2.31}$$

Such $G_o(s)$ is called the outer function, and since it does not have an unstable zero, it is stable and has the same gain as the original system. On the other hand, $G_i(s)$ is called an inner function, and if the original system $G(S)$ has an unstable zero, $G_i(s)$ also has an unstable zero. Note that $G_i^T(-s)G(s) = I_p$ holds. In MIMO systems, the Riccati equation is often used when performing inner / outer decomposition. The Riccati equation is also used in this study.

The Riccati equation used in the following discussion is defined as follows.

The target system for inner / outer decomposition is defined by Eq. (2.32).

$$M(s) = \left[\begin{array}{cc|c} A_{11} & A_{12} & B_1 \\ \hline 0 & A_{22} & B_2 \\ \hline C_1 & C_2 & D \end{array} \right] \left[\begin{array}{cc|c} A_{11} & A_{12} & B_1 \\ \hline 0 & A_{22} & B_2 \\ \hline C_1 & C_2 & D \end{array} \right] \tag{2.32}$$

At this time, the following Riccati equation has a real number solution for $M(s)$.

$$X(A_{22} - B_2D^+C_2) - (A_{11} - B_1D^+C_1)X - XB_2D^+C_1X - (A_{12} - B_1D^+C_2) = 0 \tag{2.33}$$

Hereafter, $\text{Ric}(M(s))$ refers to Eq. (2.33).

Also, when the target system $M_d(s)$ is given in the descriptor format, the extended Riccati equations $\text{ERic}(M_d(s))$ in Eqs. (2.35) and (2.36) have real number solutions X and Y .

$$M_d(s) = \left\{ \left[\begin{array}{cc} E_{11} & E_{12} \\ 0 & E_{22} \end{array} \right], \left[\begin{array}{cc|c} A_{11} & A_{12} & B_1 \\ \hline 0 & A_{22} & B_2 \\ \hline C_1 & C_2 & I \end{array} \right] \left[\begin{array}{cc|c} A_{11} & A_{12} & B_1 \\ \hline 0 & A_{22} & B_2 \\ \hline C_1 & C_2 & I \end{array} \right] \right\} \tag{2.34}$$

$$YE_{22} - E_{11}X - E_{12} = 0 \tag{2.35}$$

$$Y(A_{22} - B_2C_2) - (A_{11} - B_1C_1)X - YB_2C_1X - (A_{12} - B_1C_2) = 0 \tag{2.36}$$

When the extended Riccati equation is used in the inner-outer decomposition, $X = Y^T$.

If the number of inputs and outputs is the same and there is no invariant zero on the imaginary axis, standard spectral decomposition can be used. The target for standard spectral decomposition is defined by Eq. (2.37).

$$G(s) = \left[\begin{array}{c|c} A & B \\ \hline C & D \end{array} \right] \left[\begin{array}{c|c} A & B \\ \hline C & D \end{array} \right] \tag{2.37}$$

At this time, each character is as follows.

$$\begin{aligned} A &\in \mathbb{R}^{n \times n} \\ B &\in \mathbb{R}^{n \times p} \\ C &\in \mathbb{R}^{m \times n} \\ D &\in \mathbb{R}^{m \times p} \end{aligned}$$

The following assumptions are made in performing spectral decomposition.

- Assumption 1: $G(s)$ has no unstable pole, that is, A is stable.
- Assumption 2: D is the full rank of the column, and $\text{rank}(D) = p$ is satisfied.
- Assumption 3: $G(s)$ does not have an invariant zero on the imaginary axis.
- Assumption 4: $G(s)$ is stable.

For equation (2.37), when $G^{\sim}(s) = G^T(-s)$ is defined, $S(s)$ that satisfies the following equation is called a spectral factor, and $\text{Re}(s) < 0$ holds.

$$G^{\sim}(s)G(s) = S^{\sim}(s)S(s) \tag{2.38}$$

Expanding the left side of equation (2.38) yields equation (2.39).

$$M(s) = \left[\begin{array}{c|c} -A^T & -C^T \\ \hline B^T & D^T \end{array} \right] \left[\begin{array}{c|c} A & B \\ \hline C & D \end{array} \right] = \left[\begin{array}{cc|c} -A^T & -C^T C & -C^T D \\ \hline 0 & A & B \\ \hline B^T & D^T C & E \end{array} \right] \left[\begin{array}{c|c} -A^T & -C^T \\ \hline B^T & D^T \end{array} \right] \left[\begin{array}{c|c} A & B \\ \hline C & D \end{array} \right] = \left[\begin{array}{cc|c} -A^T & -C^T C & -C^T D \\ \hline 0 & A & B \\ \hline B^T & D^T C & E \end{array} \right]$$

However, $E = D^T D$, and the assumption 2 becomes an invertible matrix. The solution X is obtained by solving $\text{Ric}(M(s))$. Using this solution, we obtain Eq. (2.40), which means the outer function.

$$S(s) = \left[\begin{array}{c|c} A & B \\ \hline E^{-\frac{1}{2}}(D^T C + B^T X) & E^{-\frac{1}{2}} \end{array} \right] \left[\begin{array}{c|c} A & B \\ \hline E^{-\frac{1}{2}}(D^T C + B^T X) & E^{-\frac{1}{2}} \end{array} \right] \tag{2.40}$$

The state-space model of the flexible manipulator created this time has the characteristics (i) (ii) (iii) shown in 2.4.1. Therefore, inner / outer decomposition using standard spectral decomposition cannot be performed. Therefore, we perform singular spectral decomposition that includes an invariant zero on the imaginary axis that includes the point at infinity and may have $\text{rank}(D) < p$.

The target system is Eq. (2.37), and the assumptions are as follows.

- Assumption 5: $G(s)$ has no unstable pole, that is, A is stable.
- Assumption 6: $\text{rank}(D) < p$ is satisfied.
- Assumption 7: $G(s)$ is stable.

Where the spectral factor $S(s)$ that satisfies Eq. (2.38) plays the role of the outer function. Also, $S(s)$ is p input and p output.

The target system handled here includes the case of $D = 0$. Therefore, it is necessary to discuss in a descriptor format that can describe a non-proper system. When Eq. (2.38) is extended to the descriptor format, it becomes Eq. (2.41) as follows.

$$G^{\sim}(s)G(s) = \left\{ \begin{bmatrix} E_a^T & 0 \\ 0 & E_a \end{bmatrix}, \left[\begin{array}{cc|c} -A_a^T & -Q_a & 0 \\ 0 & A_a & B_a \\ \hline B_a^T & 0 & I_p \end{array} \right] \left[\begin{array}{cc|c} -A_a^T & -Q_a & 0 \\ 0 & A_a & B_a \\ \hline B_a^T & 0 & I_p \end{array} \right] \right\} \quad (2.41)$$

Where, each matrix is as follows.

$$Q_a = \begin{bmatrix} C^T C & C^T D \\ D^T C & D^T D - I_p \end{bmatrix}, E_a = \begin{bmatrix} I_n & 0 \\ 0 & 0 \end{bmatrix}$$

$$A_a = \begin{bmatrix} A & B \\ 0 & I_p \end{bmatrix}, B_a = \begin{bmatrix} 0 \\ -I_p \end{bmatrix}$$

This time, since $\text{ERic}(G^{\sim}(s)G(s))$ is used for the inner outer decomposition, there is a real number solution X such that $Y = X^T$, and the following is the outer function.

$$G_o(s) = \left\{ E_a, \left[\begin{array}{c|c} A_a & B_a \\ \hline B_a^T X & I_p \end{array} \right] \left[\begin{array}{c|c} A_a & B_a \\ \hline B_a^T X & I_p \end{array} \right] \right\} \quad (2.42)$$

2.4.4 Inverse system configuration method

The outer function $G_o(s)$ obtained from the inner outer decomposition by the singular spectrum decomposition shown in 2.4.3 is used as a linear time-invariant system of p input and p output and is given by Eq. (2.43).

$$G_o(s) = \left[\begin{array}{c|c} A & B \\ \hline C & D \end{array} \right] \left[\begin{array}{c|c} A & B \\ \hline C & D \end{array} \right] \quad (2.43)$$

Where each character is as follows.

$$A \in \mathbb{R}^{n \times n}$$

$$B \in \mathbb{R}^{n \times p}$$

$$C \in \mathbb{R}^{p \times n}$$

$$D \in \mathbb{R}^{p \times p}$$

Where, the control object this time has the same number of inputs and outputs, that is, $p = m$ and $\det(D) \neq 0$.

When $G_o(s)$ is expressed by the equation of state, it becomes Eq. (2.44).

$$G_o(s) = \begin{cases} \dot{x}(t) = Ax(t) + Bu(t) \\ y(t) = Cx(t) + Du(t) \end{cases} \quad (2.44)$$

The following equation is obtained by transforming the following equation of equation (2.44).

$$u(t) = D^{-1}\{y(t) - Cx(t)\} = -D^{-1}Cx(t) + D^{-1}y(t) \quad (2.45)$$

Substitute Eq. (2.45) into the above equation of Eq. (2.44).

$$\dot{x}(t) = Ax(t) + B\{-D^{-1}Cx(t) + D^{-1}y(t)\} = (A - BD^{-1}C)x(t) + BD^{-1}y(t) \quad (2.46)$$

From the above equations (2.45) and (2.46), the state space model of the inverse system becomes equation (2.47).

$$\hat{G}(s) = G_o^{-1}(s) = \begin{bmatrix} \hat{A} & \hat{B} \\ \hat{C} & \hat{D} \end{bmatrix} \begin{bmatrix} \hat{A} & \hat{B} \\ \hat{C} & \hat{D} \end{bmatrix} \tag{2.47}$$

Where, the parameters are as follows.

$$\begin{aligned} \hat{A} &= (A - BD^{-1}C) \\ \hat{B} &= BD^{-1} \\ \hat{C} &= -D^{-1}C \\ \hat{D} &= D^{-1} \end{aligned}$$

Here, the created inverse system is created from a linear model, but the actual flexible manipulator is an infinite dimensional system. The linear model ignores the transmission characteristics of the higher-order vibration mode, and there is a possibility that spillover will occur in which the higher-order vibration mode, which is not considered during control, causes excitation. Therefore, the inverse system this time is a low-pass type inverse system that suppresses high-order vibration with a low-pass filter and maintains internal stability. The low-pass filter is expressed by the following transfer function and connected in series as shown in Fig. 2.16. Let f_c be the cutoff frequency.

$$H(s) = \frac{1}{\frac{1}{2\pi f_c} s + 1} \tag{2.48}$$

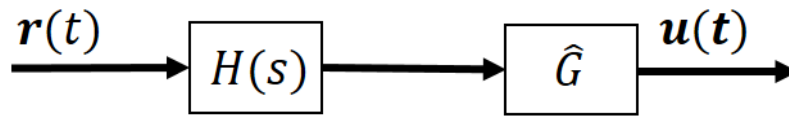


Fig. 2.16 Stable filtered inverse system.

2.4.5 Characteristics of inverse system

Evaluate the inverse system created by using the eigen decomposition and the inverse system construction method described so far. As in 2.4.1, the frequency characteristics and the pole-zero arrangement are used for the evaluation. The cutoff frequency of the low-pass filter expressed by the equation (2.48) connected in series with the inverse system was set to $f_c = 50$ [Hz].

Then, the inverse system is evaluated from the polar zero arrangement. Fig. 2.23 shows the pole-zero arrangement of the controlled system and the inverse system, and Fig. 2.24 shows an enlarged table near the origin. Red points to the poles and zeros of the linear model, and blue points to the poles and zeros of the inverse system. It can be seen that the pole of the inverse system is stable because it exists on the left side of the imaginary axis, and that the inverse system cancels the pole of the controlled system. It is considered that the new poles are generated in the inverse system because the zero point that existed at the point at infinity returned to the vicinity of the origin by reversing the function. In addition, it can

be inferred that the peak near 2 [Hz] that occurred in the Bode diagram is caused by the newly generated pole with $\text{Re}(s) \approx -13$ that can be confirmed in Fig. 2.24.

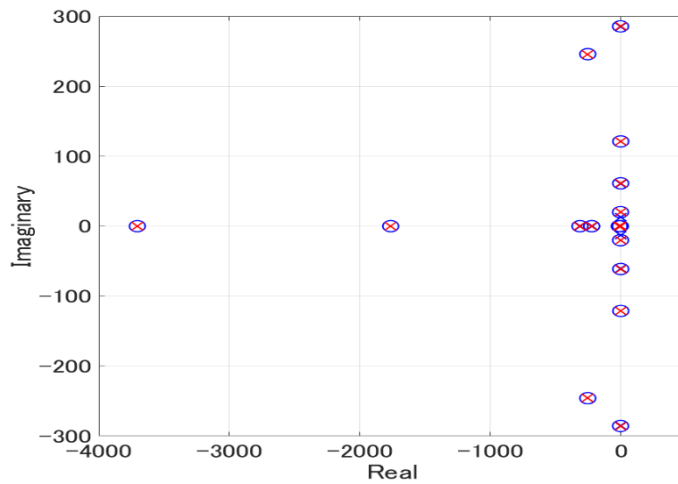


Fig. 2.23 Pole-Zero plot with inverse system.

2.5 Conclusion

In this chapter, we first described the configuration of the flexible manipulator that is the control object. Next, we created nonlinear and linear models using MaplesimTM and considered their validity and the characteristics of the models. As a result, it was found that the model has angular response and vibration characteristics close to those of the control object and has some properties to be considered when performing inner / outer decomposition. Next, after describing the singular spectral decomposition to which the inner and outer decomposition of this linear model can be applied, the controller was constructed using the inverse system configuration. As a result of considering the characteristics of the inverse system, it was confirmed that it can have vibration suppression performance while maintaining sufficient angular response performance.

In the next chapter, the performance of the controller will be evaluated by simulating and implementing the inverse system constructed in this chapter on the actual manipulator.

Chapter 3 Experiment 1 (Verification of inverse system performance)

3.1 Introduction

In this chapter, as a performance verification of the inverse system constructed in the previous chapter, a simulation using a nonlinear model and a linear model is first performed. The simulation targets a nonlinear model obtained by converting the model created by MaplesimTM into an S-function block, and a linear model generated from the nonlinear model. After that, a mounting experiment on the actual manipulator is performed to verify the performance. The experimental method is to input a 20 [deg] square wave to each motor described in Chapter 2.

3.2 Simulation results and consideration

The simulation results are shown in Fig. 3.1 to Fig. 3.6. Fig. 3.1 and Fig. 3.4 are the angular response of each joint, Fig. 3.2 and Fig. 3.5 are the distortion FFT results, and Fig. 3.3 and Fig. 3.6 are the distortion FFT results.

It can be seen that both the non-linear model and the linear model have sufficient tracking performance in the angular response, and the overshoot, which remains a problem in the conventional research, is suppressed. In the simulation, vibration is generated in the angular response, but in the actual motor, the vibration is reduced. This is thought to be caused by the viscosity, friction, and reduced responsiveness generated in the motor.

Next, we will consider the vibration suppression performance. In the linear model, it can be seen that vibration can be suppressed at peaks near 3 [Hz], 10 [Hz], and 20 [Hz]. It is considered that the newly appearing peak near 2 [Hz] is caused by the pole generated when the infinite zero converges near the origin when the equation for constructing the inverse system is solved. In the nonlinear model, the vibration is not suppressed near 10 [Hz] and 20 [Hz], but in the actual manipulator, the damping is larger than that of the model, so it is considered that there is no big influence. It is considered that the vibration of the high frequency component generated in the actual manipulator can be suppressed by the strain feedback dealt with in a later chapter. In the nonlinear model, the vibration suppression effect is smaller after 10 [s] for both Link1 and Link2 strains, that is, when returning to the initial posture, compared to before 10 [s]. Let us consider this. In the state space model, the initial value is one important parameter. The linear model used this time uses the attitude at the start time as the initial value, and the attitude at 10 [s] is different from the properties of the control object. Therefore, it is considered that the effect of canceling the vibration characteristics by the inverse system was not sufficiently exhibited, and the vibration suppression performance was deteriorated.

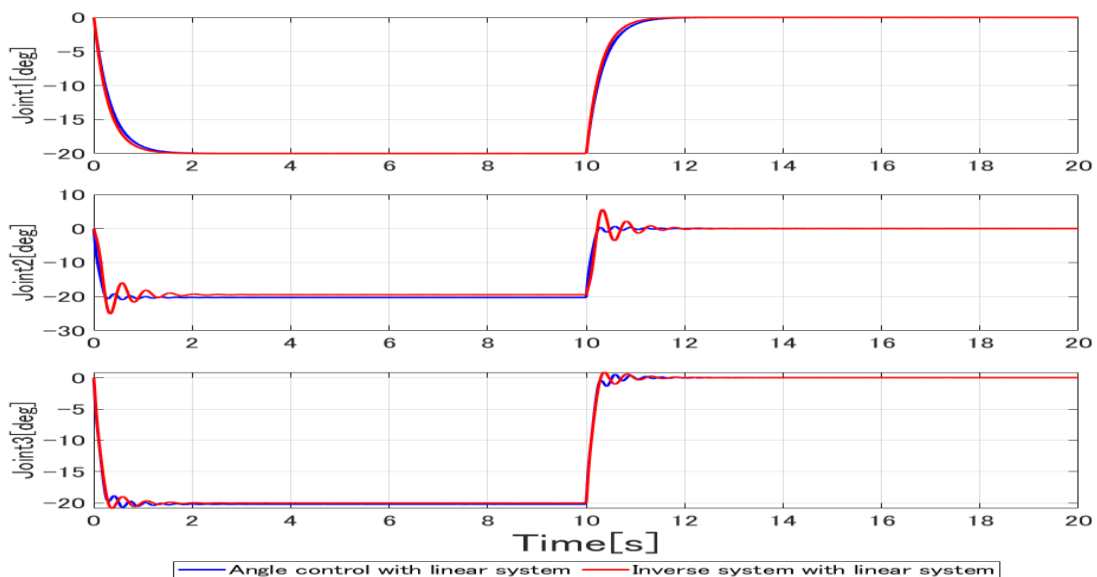


Fig. 3.4 Angle response of linear model with inverse system.

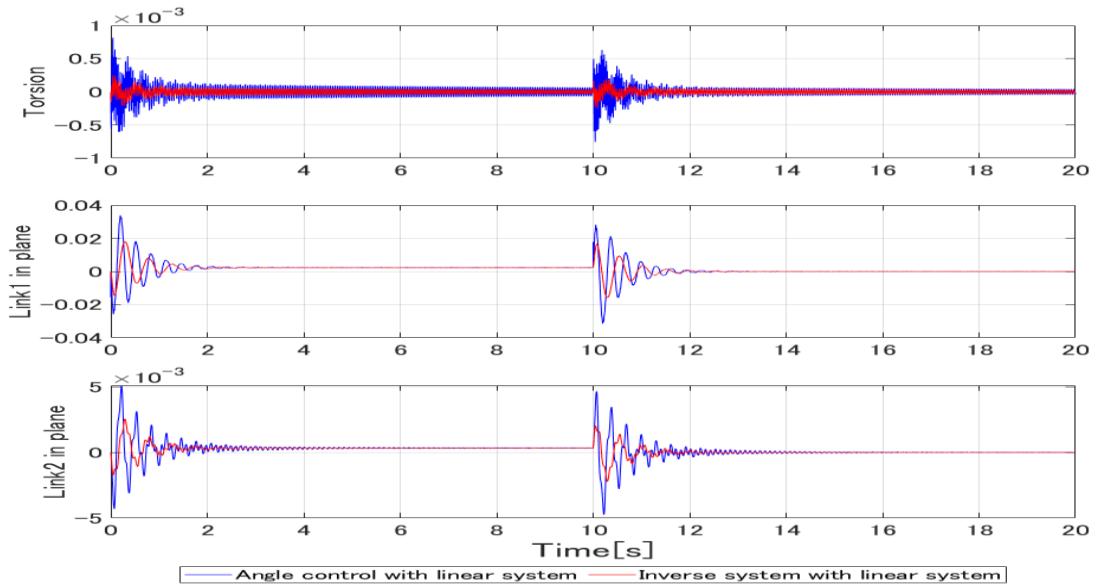


Fig. 3.5 Strain of linear model with inverse system.

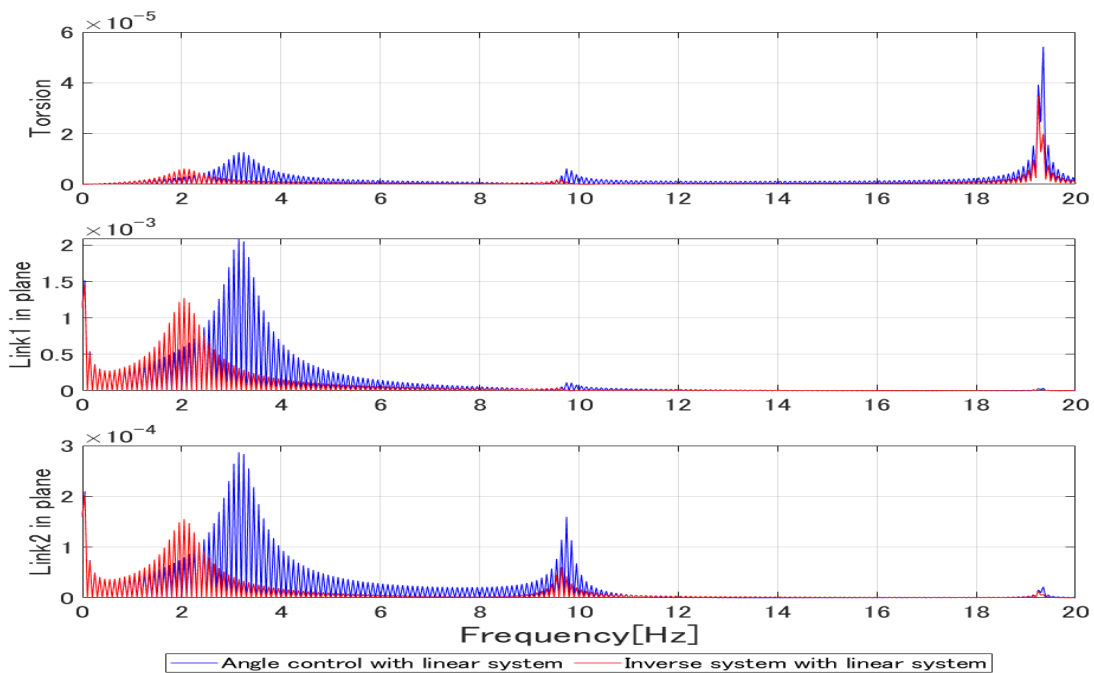


Fig. 3.6 FFT of linear model with inverse system.

3.3 Implementation experiment and consideration

In the above simulation, it was confirmed that the non-linear model and the linear model do not overshoot, which was the subject of conventional research, while maintaining sufficient tracking performance to the target angle. Here, the proposed method of control by the inverse system is performed on the actual manipulator. Performance is evaluated by comparison with the inverse system proposed in the previous research.

The experimental results on the actual manipulator are shown in Fig. 3.7 to Fig. 3.9. Regarding the

angular response, in the conventional method, overshoot occurs in all Joints, whereas in the proposed method, it converges without exceeding the target value. In addition, it can be seen that the proposed method approaches faster in the convergence to the target angle.

Regarding the vibration, it can be seen that the vibration in the in-plane direction is improved, especially for the resonance frequency component of 3 [Hz], as compared with the conventional proposed method. It can also be seen that in the torsional and out-of-plane directions, the vibration from immediately after the start to 10 [s] is suppressed by the inverse system of the proposed method.

From the above, it can be seen that the proposed method is superior in terms of angle control accuracy and vibration suppression performance when it is assumed that it will be used as a manipulator.

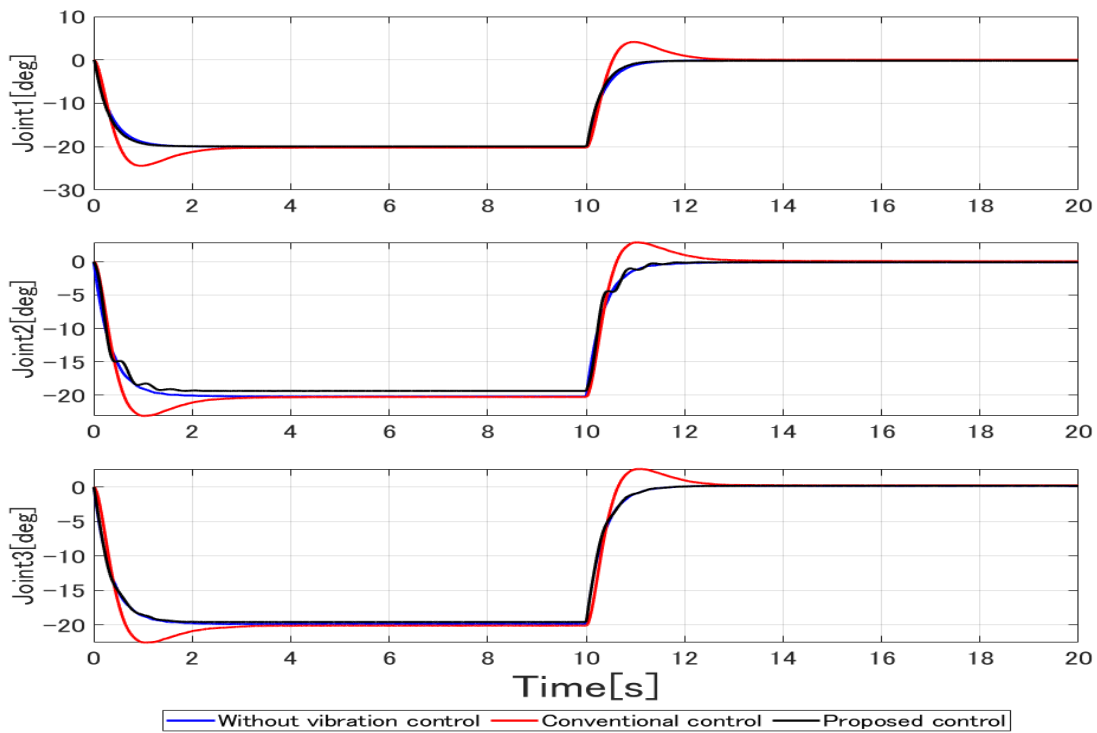


Fig. 3.7 Angle response of actual manipulator with inverse system.

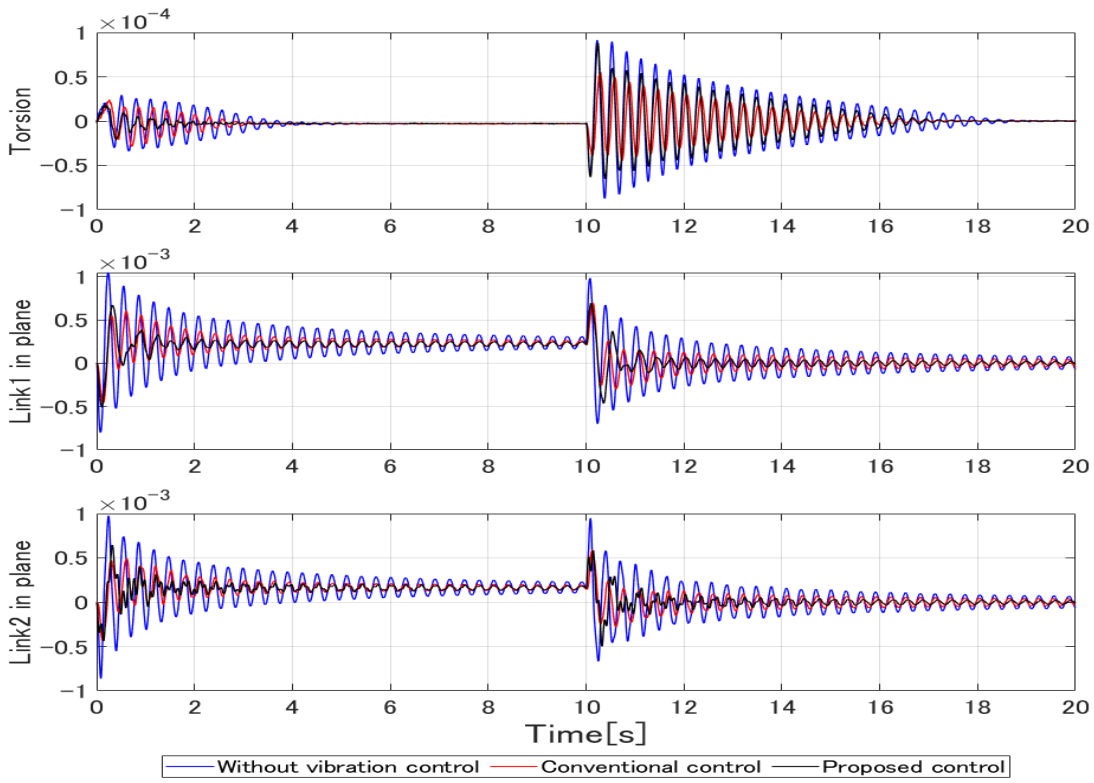


Fig. 3.8 Strain response of actual manipulator with inverse system (torsion and in planes).

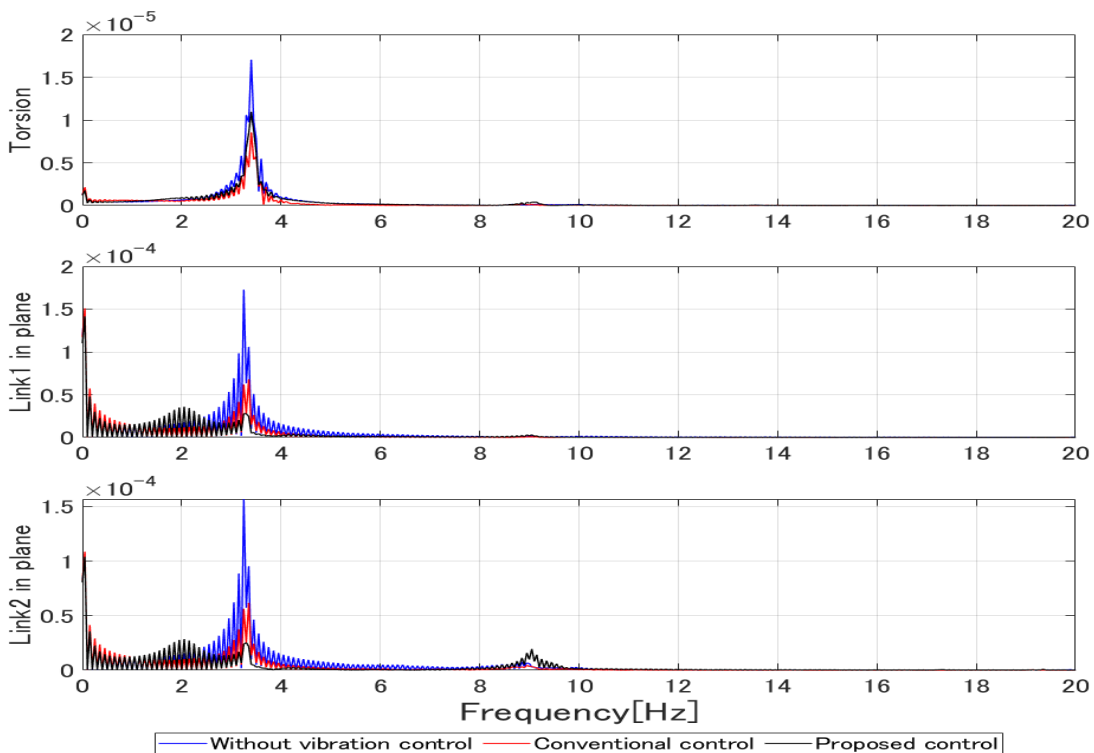


Fig. 3.9 FFT of actual manipulator with inverse system (torsion and in planes).

3.4 Conclusion

In this chapter, the performance of the inverse system, which is the proposed method, was verified by

simulation and implementation experiment on the actual flexible manipulator.

In the simulation, it was confirmed that the inverse system of the proposed method has sufficient tracking performance to the target angle and is effective against torsion and in-plane vibration.

Subsequently, it was found that the mounting experiment on the actual manipulator was superior to the conventional research in terms of the speed of angular response, the presence or absence of overshoot, and the vibration suppression performance.

Chapter 6 Conclusion

In this study, we constructed a control system using an inverse system for the purpose of suppressing 3D vibration of a flexible manipulator with 2 links and 3 degrees of freedom and verified its performance by simulation and mounting experiments on an actual manipulator.

First, we created a linear model of the flexible manipulator and summarized the properties of that model. Since the linear model used this time was found to be a system with invariant zeros on the imaginary axis including the point at infinity, the input and output are different, so singular spectral decomposition was used for the inner and outer decomposition. An inverse system was created based on the outer function created in this way, and the characteristics were evaluated from the frequency response and the pole-zero arrangement, and it was confirmed that it has effective properties for vibration suppression. Subsequently, the performance of the inverse system was verified by simulation and implementation experiment on the actual manipulator. As a result, it was confirmed that the overshoot, which remained as an issue in the conventional research, was suppressed, and the vibration suppression performance for the resonance frequency component near 3 [Hz] was improved.

From the above, it can be said that the control system using the inverse system is effective for a flexible manipulator with 2 links and 3 degrees of freedom that moves in 3 dimensions.

Acknowledgement

This work is partially supported by Grants-in-aid for Promotion of Regional Industry-University-Government Collaboration from Cabinet Office, Japan

References

- [1] Makoto Kaneko, "Special Feature on Flexible Arms", Journal of the Robotics Society of Japan, Vol.6, No.5, pp. 414-466 (1988).
- [2] Fumitoshi Matsuno, Special Issue on "Flexible Manipulators", Journal of the Robotics Society of Japan, Vol.12, No.2, pp. 169-230 (1994).
- [3] Toshio Fukuda, Control of flexible robot arm: 1st report, Vibration control during positioning of 1st and 2nd degree of freedom system, Proceedings of the Japan Society of Mechanical Engineers C, 1985, 51, 468, pp. 2140-2144.
- [4] Toshio Fukuda, Atsushi Arakawa, Control of flexible robot arm: 2nd report, Modeling and basic characteristics of 2-degree-of-freedom coupled system, Proceedings of the Japan Society of Mechanical

Engineers C, 1987, 53, 488, pp. 954-961.

[5] Atsushi Arakawa, Toshio Fukuda, Control of Flexible Robot Arm: 3rd Report, Optimal Vibration Suppression Control and Sensitivity Analysis of 3 Degrees of Freedom System, Proceedings of the Japan Society of Mechanical Engineers C, 1990, Vol. 56, No. 529, pp. 2446-2453.

[6] Masaka Luo, Theoretical and Experimental Consideration of Control of Flexible Robot Arm by Strain Feedback, Proceedings of the Society of Instrument and Control Engineers, 1992, Vol. 28, No. 1, pp. 67-76.

[8] Isao Yamada, Construction method of inverse system and its application to manufacturing, Measurement and control, 1997, Vol. 36, No. 6, pp. 417-425.

[9] Hiroshi Okajima, Instability Zero and Control, System / Control / Information, 2020, Vol. 64, No. 9, pp. 349-354.

[10] Isao Yamada, Ko Kinoshita, New Design Method for Stable Low-pass Inverse System by State Space Method and Its Application, Journal of the Society of System Control and Information Science, 2003, Vol. 16, No. 2, pp. 85-93.

[11] Masaya Tanemura, Yuichi Senda, Design of parallel feedforward compensator using descriptor format and improvement of disturbance estimation performance of non-minimum phase system, Proceedings of Society of Instrument and Control Engineers, 2018, Vol. 54, No. 4, pp. 402-411.

[12] Isao Yamada, Construction method of low-pass stable inverse system and application to inner / outer decomposition for truly proper system, IEEJ Transactions on Electronics, Information and Systems, 2000, 120, No. 11, pp. 1711-1719.

[13] Masayuki Sato, A design method for low-pass inverse systems, Proceedings of the Society of Instrument and Control Engineers, 2000, Vol. 36, No. 12, pp. 1180-1182.

[14] Akira Satoshi, Zenta Iwai, Ikuo Mizumoto, Simple Adaptive Control System Design for Process Systems with Uncertainty, Proceedings of the Society of Instrument and Control Engineers, 1999, Vol. 35, No. 7, pp. 852-860.

[15] Hiroshi Okajima, Instability Zero and Control, System / Control / Information, 2020, Vol. 64, No. 9, pp. 349-354.

[16] Isao Yamada, Keiji Watanabe, Construction method of stable low-passing inverse system by state-space method, Proceedings of the Society of Instrument and Control Engineers, 1996, Vol. 32, No. 6, pp. 862-870.

[17] Wang Bao, Keiji Watanabe, Kenichi Muramatsu, Yuichi Ariga, Shigeru Endo, Design of a stable inverse system for a reversible system with an unstable zero in the state space, Journal of the Society of Systems Control and Information Science, 2006, 19, No. 7, pp. 290-292.

[18] Yoshiaki Asahi, Keiji Watanabe, Kenichi Muramatsu, Yuichi Ariga, Systematic design method of non-interference for non-minimum phase system by state feedback and inverse system, Proceedings of the Society of Instrument and Control Engineers, 2005, Vol. 41, No. 3, Pp. 234-241.

[19] Njeri, W., Sasaki, M. & Matsushita, K. Enhanced vibration control of a multilink flexible

manipulator using filtered inverse controller. *Robomech J* 5, 28 (2018).

[20] Njeri, W., M. Sasaki and K. Matsushita, "Two-degree-of-freedom control of a multilink flexible manipulator using filtered inverse feedforward controller and strain feedback controller," 2018 IEEE International Conference on Applied System Invention (ICASI), 2018, pp. 972-975.

[21] Njeri, W., M. Sasaki and K. Matsushita, Gain Tuning for High-Speed Vibration Control of a Multilink Flexible Manipulator Using Artificial Neural Network. *Journal of Vibration and Acoustics*. 141. 1. 10.1115 / 1.4043241.

[22] A. Emami-Naeini, P. Van Dooren, Computation of zeros of linear multivariable systems
Volume 18, Issue 4, July 1982, pp. 415-430.

[23] Qingze Zou, "Optimal preview-based stable-inversion for output tracking of nonminimum-phase linear systems," 2007 46th IEEE Conference on Decision and Control, 2007, pp. 5258-5263.

[24] George, KK., Verhaegen, MHG., & Scherpen, JMA, 1999, Stable inversion of MIMO linear discrete time non-minimum phase systems. In *MED99 Proceedings*, pp. 267-281.

[25] Gou Ichimasa, Hiroshi Okajima, Kosuke Okumura & Nobutomo Matsunaga, 2017, Model Error Compensator with Parallel Feed-Forward Filter, *SICE Journal of Control, Measurement, and System Integration*, 10: 5, pp. 468-475.

[26] Oara, Cristian & Varga, Andras, 2001, Computation of General Inner-Outer and Spectral Factorizations, *Automatic Control, IEEE Transactions on*. 45. pp. 2307 --2325.

[27] Shinji Hara, Toshiharu Sugie, Inner-outer factorization for strictly proper functions with $j\omega$ -axis zeros, *Systems & Control Letters*, Volume 16, Issue 3,1991, Pages 179-185.

[28] Tsutomu Mita, Kazunobu Kuriyama, << Part 2 >> Decomposition of transfer functions, spectral decomposition and Riccati equations, *measurement and control*, 1996, Vol. 35, No. 6, pp. 467-476.

[29] Kazunobu Kuriyama, Tsutomu Mita, Decomposition theory of rational function matrix by descriptor expression and its application to spectral decomposition, *Proceedings of the Society of Instrument and Control Engineers*, 1995, Vol. 31, No. 3, pp. 315-323.

[30] Yasuyuki Funahashi, Satoko Yamakawa, Zero-point elimination condition and strong stabilization law by 2-delay output control, *Proceedings of the Society of Instrument and Control Engineers*, 1995, Vol. 31, No. 1, p. 48-55.